PERGAMON

Computers & Fluids 31 (2002) 481–494

computers & fluids

www.elsevier.com/locate/compfluid

Numerical investigation of the first bifurcation for the flow in a rotor–stator cavity of radial aspect ratio 10

O. Daube *, P. Le Quéré

LIMSI-CNRS, BP 133, 91403 Orsay Cedex, France

Received 1 August 2001

Abstract

The nature of transition to unsteadiness of rotor–stator disk flows of large radial aspect ratio is investigated by means of several numerical tools which consist in computing the base flow even when unstable, performing linearized or non-linear time integrations starting from initial conditions of different amplitudes and computing the spectrum of the Jacobian using the ARPACK library. From these numerical experiments we conclude that, in a cavity of radial aspect ratio 10, the transition to unsteadiness occurs through a subcritical Hopf bifurcation. In addition these calculations show the existence of a large amplitude chaotic branch for values of the Reynolds number far below the linear stability threshold, and onto which the solutions are attracted for large subcritical values due to the strong non-normality of the Jacobian of the evolution operator. © 2002 Elsevier Science Ltd. All rights reserved.

Keywords: Rotor–stator disk flow; Hopf bifurcation; Subcriticality; Non-normality

1. Introduction

We have been studying flows in cylindrical enclosures for more than a decade now. Over the last few years we have been particularly interested in flows which occur between two disks of large radial extend compared to their spacing with one rotating disk and the other one at rest, the so-called rotor–stator configuration, a configuration that occurs in many problems of engineering interest [1–4]. For many applications the typical lengths or rotational rates are large enough that the corresponding flow is turbulent and there are thus engineering needs to dispose of numerical

* Corresponding author. Present address: CEMIF, 40 rue du Pelvoux, CE 1455, Courcouronnes, 91020 Evry Cedex, France.

PII: S0045-7930(01)00059-7

tools able to quantitatively predict the corresponding flow structure and related heat transfer for the purpose of optimization.

Our primary goal was to perform some DNS and LES computations which could be used to assess RANSE models available in the literature for this kind of flows [5]. In order to validate our numerical methodologies, we first wanted to perform computations for rotational Reynolds numbers corresponding to transition to unsteadiness. From our experience in natural convection flows [6] and flows in a tank with a rotating lid [7], we expected to find first a critical Reynolds number beyond which the flow would become nicely mono-periodic and then successive bifurcations ultimately leading to chaos. Surprisingly, or maybe not so much afterwards, we did not observe this scenario and we spent much time and work to try to explain this behavior [8] that we first tentatively ascribed to two reasons: we suspected that this pathological behavior could be due either to the singularity in $r = 0$ or to the discontinuity in the boundary conditions. Actually none of these reasons turned out to be able to explain what we observed and we therefore decided to look for another possible cause, namely that the bifurcation could be subcritical. This paper is devoted to the report of our latest numerical experiments aimed at investigating this possibility for one particular configuration, namely a rotor–stator cavity of $A = 10$ with the shroud attached to the rotating disk. This configuration was chosen because it seems to be representative of the phenomena which occur in rotor–stator flows.

The paper is organized as follows. In the first two sections, we first recall the configuration and its governing equations and the main features of the numerics are outlined. Then, the observations from our first computations concerning the transition to unsteadiness are reported. They can be summarized by:

- We did get a Reynolds number beyond which the flow becomes unsteady.
- This unsteadiness is apparently of quasi-periodic type or chaotic type.
- No appreciable hysteresis could be observed.

A linear stability analysis is then performed which evidences some characteristic features of these flows, in particular the existence of a linear critical Reynolds number and the subcritical nature of the associated bifurcation, a feature which is probably related to the strongly non-normal character of the Jacobian operator. Finally, some eigenmodes computations are shown which confirm the previous results.

2. Problem definition and equations

In this paper, we are interested in the axisymmetric flow in a cylindrical cavity of large radial aspect ratio $A = R_0/H$, generated by the rotation at a constant angular velocity Ω of one of the disks and of the outer shroud (see Fig. 1). The axisymmetric Navier–Stokes equations in a meridional plane $[0 \leqslant r \leqslant A] \times [0 \leqslant z \leqslant 1]$ are cast in the so-called ψ–ω formulation which makes use of the stream function ψ and of the vorticity function ω. Some other calculations were performed using the primitive variables and a pseudo-spectral method. Quite similar results were obtained and therefore, only the ψ–ω formulation will be presented here. In cylindrical coordinates (r, z), the axisymmetric incompressible NS equations read:

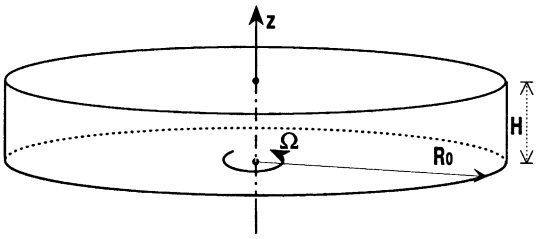

$$\mathrm{Re} = \frac{\Omega H^2}{\nu} \qquad A = \frac{R_0}{H}$$

Fig. 1. Sketch of the configuration.

$$\frac{\partial\omega}{\partial t}+\frac{\partial(u\omega)}{\partial r}+\frac{\partial(w\omega)}{\partial z}-\frac{\partial}{\partial z}\left(\frac{v^2}{r}\right)=\frac{1}{Re}\left(\frac{\partial}{\partial r}\left(\frac{1}{r}\frac{\partial(r\omega)}{\partial r}\right)+\frac{\partial^2\omega}{\partial z^2}\right) \tag{1}$$

$$\frac{\partial v}{\partial t}+\frac{\partial(uv)}{\partial r}+\frac{\partial(wv)}{\partial z}+2\frac{uv}{r}=\frac{1}{Re}\left(\frac{\partial}{\partial r}\left(\frac{1}{r}\frac{\partial(rv)}{\partial r}\right)+\frac{\partial^2 v}{\partial z^2}\right) \tag{2}$$

$$\frac{\partial}{\partial r}\left(\frac{1}{r}\frac{\partial\psi}{\partial r}\right)+\frac{1}{r}\frac{\partial^2\psi}{\partial z^2}=\omega \tag{3}$$

where u and w are the radial and axial components of the solenoidal velocity field, related to the stream function and the vorticity function by:

$$u=\frac{1}{r}\frac{\partial\psi}{\partial z};\quad w=-\frac{1}{r}\frac{\partial\psi}{\partial r};\quad \omega=\frac{\partial u}{\partial z}-\frac{\partial w}{\partial r}$$

The boundary conditions concern only the velocity and are of Dirichlet type as usual. From the no-slip conditions for u and w, the classical conditions on ψ are derived:

$$\psi=0 \quad \text{on } r=0;\ r=A;\ z=0;\ z=1 \tag{4}$$

$$\frac{\partial\psi}{\partial n}=0 \quad \text{on } r=0;\ r=A;\ z=0;\ z=1 \tag{5}$$

3. The numerical schemes

Before presenting the different numerical tools which are used for the purpose of this study, it may be useful to give some details on the technique we use to solve the full unsteady non-linear NS equations and which underlies most of these tools.

3.1. Time discretization

Because we are interested in stability problem in which the time accuracy is of great importance, we have chosen to use a second order time stepping scheme which ensures in particular, that the amplitude of the fluctuations around a mean state will be independent on the computational time

step, a requirement which is generally not fulfilled when using first order schemes. This second order scheme is based upon two main ingredients [9]:

1. The time derivative in the momentum equations is approximated by a second order Euler backward scheme:

$$\frac{\partial f^{n+1}}{\partial t} = \frac{3f^{n+1} - 4f^n + f^{n-1}}{2\Delta t} + \mathcal{O}(\Delta t^2)$$

2. The linear terms L are implicitly evaluated at time $(n+1)\Delta t$ whereas the non-linear part NL is explicitly evaluated at time $(n+1)\Delta t$ by means of an Adams–Bashforth extrapolation:

$$NL^{n+1} = 2NL^n - NL^{n-1}$$

This time stepping scheme yields an Helmholtz type problem for (ω^{n+1}, v^{n+1}) in which the v-equation (2) is decoupled from the vorticity transport equation:

$$(\sigma I - \nabla^2)v^{n+1} = S_v^{n,n-1} \tag{6}$$

$$(\sigma I - \nabla^2)\omega^{n+1} = S_\omega^{n,n-1} \tag{7}$$

$$r\frac{\partial}{\partial r}\left(\frac{1}{r}\frac{\partial \psi^{n+1}}{\partial r}\right) + \frac{\partial^2 \psi^{n+1}}{\partial z^2} = r\omega^{n+1} \tag{8}$$

where $\sigma = 3Re/2\Delta t$. The source terms $S_v^{n,n-1}$ and $S_\omega^{n,n-1}$ contain all the quantities which are evaluated at previous time steps.

3.2. Spatial discretization

The spatial discretization uses standard second order centered finite differences on a uniform grid, which allows us to use fast direct solvers based upon a partial diagonalization technique [10] in the z-direction to solve the resulting discrete systems. After some preliminary computations, a spatial resolution of 600×160 in (r, z) was used throughout this work, since it was found a good compromise between CPU and accuracy requirements. We are however aware that some additional grid tests should be made, and also that it may be necessary to use a non-uniform grid.

3.3. Influence matrix technique

One of the main difficulty in solving the NS equations stems from the fact that Eqs. (7) and (8) are coupled through the boundary conditions (4) and (5). This coupling is enforced as follows: once the v-equation (6) is solved, the vorticity transport equation (7) is solved a first time with an arbitrary vorticity distribution on the boundary, resulting in a stream function that does not satisfy boundary condition (5). The induced boundary tangential velocity is used through an influence matrix technique to determine a new vorticity distribution which will be used in a second resolution of Eqs. (7) and (8), therefore ensuring that the resulting solution satisfies both boundary conditions (4) and (5).

4. Transition to unsteadiness

Our first goal was to try to determine a critical Reynolds number for the onset of unsteadiness, i.e. a Reynolds number beyond which the flow would become unsteady. For this purpose, several computations were carried out in a classical way. First, the flow was computed for a sufficiently low Reynolds number, say $Re = 1000$. For this value, the flow is asymptotically steady. It is then used as an initial condition for a computation at $Re = 1600$ and so on, along the path $1600 \rightarrow 1700 \rightarrow 1800 \rightarrow 1850$. The time evolution of the maximum of the time derivative for the two last Reynolds numbers, is reported by the corresponding curves of Fig. 2. From examination of this graph, it is possible to conclude that the flow becomes unsteady for a value of the Reynolds number between 1800 and 1850.

The next step is to check if some hysteresis could be present. For this purpose, the instantaneous state which was obtained at $Re = 1850$ after 120 revolutions was in turn used as an initial condition for $Re = 1800$. As can be seen from last curve on Fig. 2 the flow then reverted to a steady state and therefore no appreciable hysteresis could be detected in the range [1800, 1850].

Maybe more important is the fact that in the course of our numerical experiments, it was never possible to observe a nice mono-periodic flow as we expected from our previous experiments with flows in a rotating tank [7] or in a differentially heated cavity [6]. Actually, as soon as the transition to unsteadiness occurred, an apparently chaotic state was obtained, whatever the initial condition which was used. This behavior may be observed on Fig. 3 which displays the time evolution of the local angular velocity v/r at three different nodes, located close to the stator at three radial positions: $R_0/5$, $2R_0/5$ and $3R_0/5$ for $Re = 1900$. These plots indicate that the flow is apparently chaotic with frequencies very different from one point to another. This may indicate a subcritical bifurcation in conjunction with the existence of a large amplitude branch, extending far below the critical linear Reynolds number. In order to investigate this assumption more precisely, we decided to carry out a linear stability of the flow. For this purpose, the first step is to compute a steady base flow.

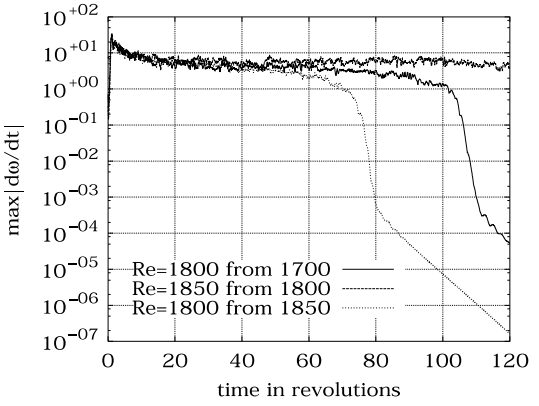

Fig. 2. Temporal evolution of $\max|\partial\omega/\partial t|$ for $Re = 1800$ and 1850.

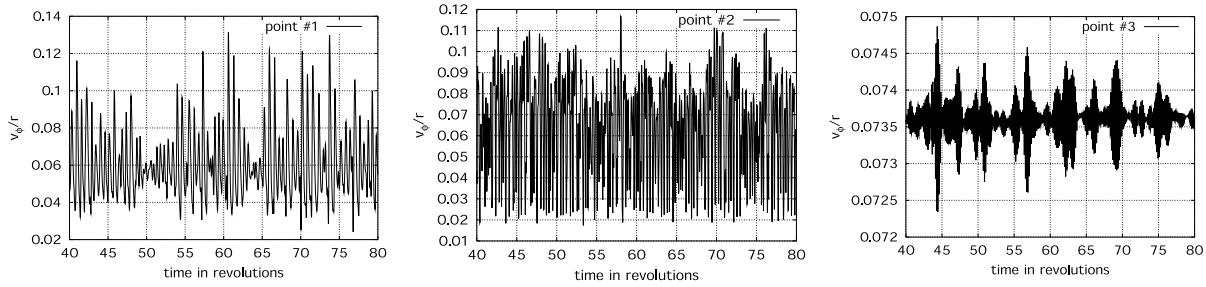

Fig. 3. Time evolution of v/r at three different locations along the stator for $Re = 1900$.

5. Computation of the base steady flows

Since our goal is to compute steady base flows, even when they are unstable, the usual procedure which consists in obtaining steady state solutions by letting $t \to \infty$ in a time stepping code must be rejected in favor of a Newton–Raphson method. The main drawback of this last approach is that the Jacobian matrix of the Navier–Stokes operator is huge and ill-conditioned. To overcome these difficulties, we have used the Stokes preconditioned Newton method which was proposed by Tuckerman [15,16]. This technique relies on two main ingredients:

(1) A time stepping code to solve the full non-linear equations and its by product to solve the linearized equations around a base flow (see Section 3).

(2) A matrix free method, such as GMRES [13], to solve the linear systems involved at each Newton iteration. These matrix free methods only require computing the action of the matrix onto a vector, which amounts in our case, to solving one time step of the linearized NS equations. This preconditioned Newton method turns out to be very efficient provided the full discrete coupled system is solved at each time step, as it is the case in this work since an influence matrix technique is used to ensure the no-slip condition. The quadratic convergence of the Newton

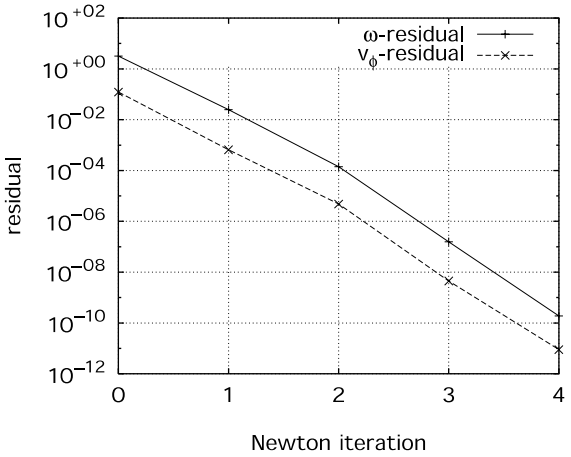

Fig. 4. Newton residual for $Re = 2000$.

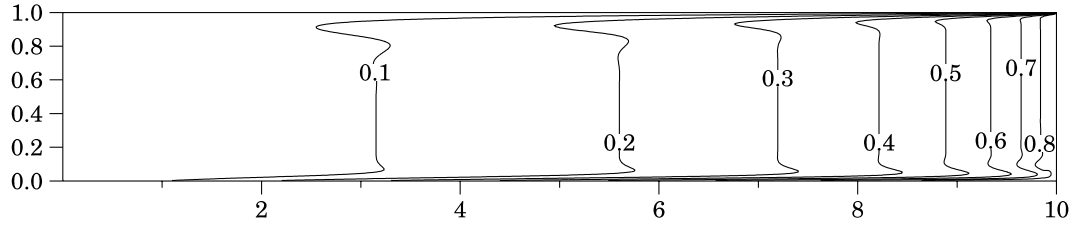

Fig. 5. Iso-v lines for $Re = 3000$.

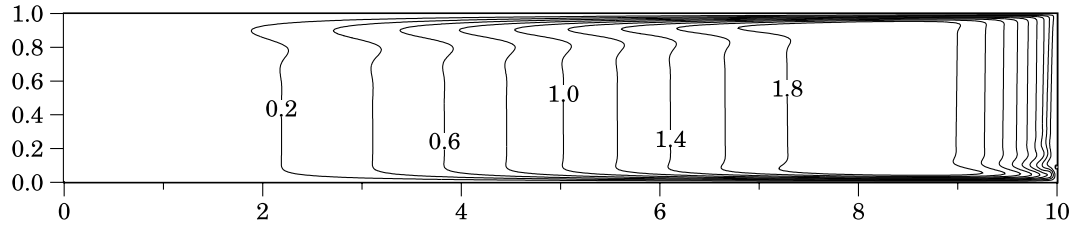

Fig. 6. Streamlines for $Re = 3000$.

method was therefore recovered as can be seen on Fig. 4 where the evolution of the residual of the non-linear NS operator is reported for $Re = 2000$.

Examples of streamlines and of iso-v lines given on Figs. 5 and 6 for $Re = 3000$ clearly show that the flow structure is of Batchelor type, i.e. with two distinct boundary layers enclosing a core which is locally in solid rotation.

Remark. From now on, both in linear and in non-linear computations, E' will denote the kinetic energy of the fluctuations around the base flow and E_0 will denote the kinetic energy of the base flow. The actual quantity of interest for our purpose is the ratio E'/E_0.

6. Linear stability analysis

Once a steady base solution $(U_b, V_b, W_b, \Omega_b)$ is computed, its linear stability is investigated by considering the fluctuations u', v' and w' of the velocity around this base solution. For this purpose, two computational approaches are used. In the first one, the linearized NS equations for u', v' and w' are considered:

$$\frac{\partial\omega'}{\partial t}+\frac{\partial(U_b\omega')}{\partial r}+\frac{\partial(W_b\omega')}{\partial z}+\frac{\partial(u'\Omega_b)}{\partial r}+\frac{\partial(w'\Omega_b)}{\partial z}-2\frac{\partial}{\partial z}\left(\frac{V_b v'}{r}\right)=\frac{1}{Re}\left(\frac{\partial}{\partial r}\left(\frac{1}{r}\frac{\partial(r\omega')}{\partial r}\right)+\frac{\partial^2\omega'}{\partial z^2}\right) \tag{9}$$

$$\frac{\partial v'}{\partial t}+\frac{\partial(U_b v')}{\partial r}+\frac{\partial(W_b v')}{\partial z}+\frac{\partial(u'V_b)}{\partial r}+\frac{\partial(w'V_b)}{\partial z}+2\frac{U_b v'+u'V_b}{r}=\frac{1}{Re}\left(\frac{\partial}{\partial r}\left(\frac{1}{r}\frac{\partial(rv')}{\partial r}\right)+\frac{\partial^2 v'}{\partial z^2}\right) \tag{10}$$

$$\frac{\partial}{\partial r}\left(\frac{1}{r}\frac{\partial \psi'}{\partial r}\right)+\frac{1}{r}\frac{\partial^2 \psi'}{\partial z^2}=\omega' \tag{11}$$

where u', v' and w' are related to the fluctuating stream function ψ' and to the fluctuating vorticity function ω' by:

$$u'=\frac{1}{r}\frac{\partial \psi'}{\partial z};\quad w'=-\frac{1}{r}\frac{\partial \psi'}{\partial r};\quad \omega'=\frac{\partial u'}{\partial z}-\frac{\partial w'}{\partial r}$$

The boundary conditions concern only the velocity and are of homogeneous Dirichlet type. These equations are integrated in time, starting from an initial small perturbation; looking at the long term time evolution the energy of the flow then permits us to tell if the flow is stable or unstable.

In the second approach, the spectrum of the linearized NS operator is computed which allows for the determination of a stability threshold, by looking at the value of the Reynolds number for which a real eigenvalue or pair of complex conjugate eigenvalues cross the imaginary axis.

6.1. Time integration of the linearized NS equations

The linearized NS equations (9)–(11) are integrated in time by means of the linearized version of our time stepping scheme. The initial conditions consists of 0 everywhere for the fluctuating stream and vorticity functions and of a random field for the azimuthal component v'. On Fig. 7 the temporal evolution of E'/E_0 is reported for $Re = 2700$, 2800, 2900 and 3000.

These diagrams display several interesting features:

(1) the critical Reynolds number beyond which the flow becomes linearly unstable, lies in the range [2900,3000]. This is much larger than the values for which the onset of unsteadiness in the non-linear computations has been observed. This a first indication of a possible subcritical nature of the bifurcation.

(2) the transient evolution of the energy may be divided in three stages:

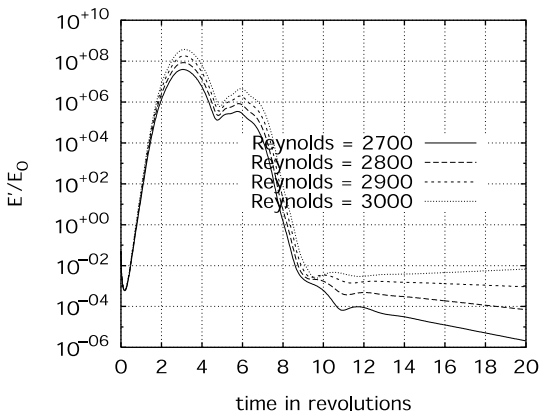

Fig. 7. Temporal evolution of the energy of the fluctuations.

- During the first four revolutions, a dramatic increase in energy occurs, by a factor as large as 10^{10} for $Re = 3000$.
- During the five next revolutions, the energy decreases down to a level which is of the same order of magnitude as the original perturbation one.
- The classical linear stage is then observed, in which an exponential evolution is recovered.

Noteworthy is the fact that a huge increase in energy occurs in the linear regime, whatever the nature—stable or unstable—of the final state. This is strongly related to the non-normality of the Jacobian operator, i.e. the eigenvectors are non-orthogonal. This point was addressed for instance by Trefethen [14].

7. Nature of the bifurcation

Since we suspected that the bifurcation which occurs between 2900 and 3000 was subcritical, we decided to integrate the full non-linear NS equations written in perturbation form around a base flow for different Reynolds numbers and for each of them, starting from various initial perturbation fields. These initial conditions were either a randomly distributed perturbation on the azimuthal component (and zero for the stream and vorticity functions) or the final state of the linear computation of Section 6.1 normalized to the desired level of kinetic energy.

7.1. Re = 3000

We remind the reader that this value is slightly supercritical. In order to detect a possible supercritical Hopf bifurcation, the amplitude of the initial perturbations was made very small in order to obtain an energy level as low as 10^{-20} times the kinetic energy of the base flow.

The temporal evolutions of the kinetic energy (normalized by the energy of the base flow) are reported on Fig. 8 for two different initial conditions. It is clearly seen that even with an initial fluctuation energy as small as (10^{-20}) times the energy of the base flow, the time integration eventually leads to an asymptotic state which is apparently chaotic and which does not depend neither on the initial energy level nor on the shape of the initial perturbation. These are indications of a likely subcritical nature of the bifurcation.

Another indication of this character may be obtained as follows:

- A linear computation is performed up to a time when the flow is in the exponential stage ($t \simeq 20$ on Fig. 7). The reached state is then scaled in order that its kinetic energy E' is $10^{-10} \times E_0$.
- This scaled final state is used as an initial condition for both linear and non-linear computations.

On Fig. 9 are displayed the time evolutions of E'/E_0 for the linear and the non-linear calculations. It can be seen that after a transient linear stage in which both curves coincide, saturation is reached through a curve with an essentially upwards concavity, a fact which reveals that the cubic term in the amplitude equation associated with this bifurcation, has a non-negative coefficient, therefore indicating its subcritical nature.

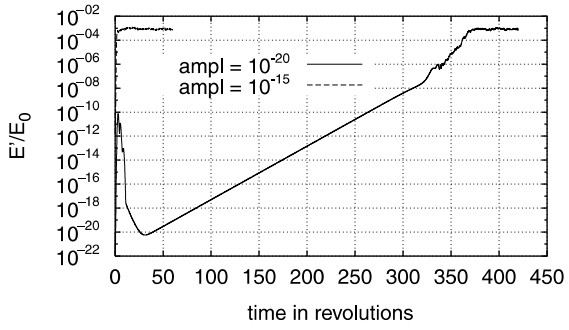

Fig. 8. Temporal evolution of the energy of the fluctuations for $Re = 3000$.

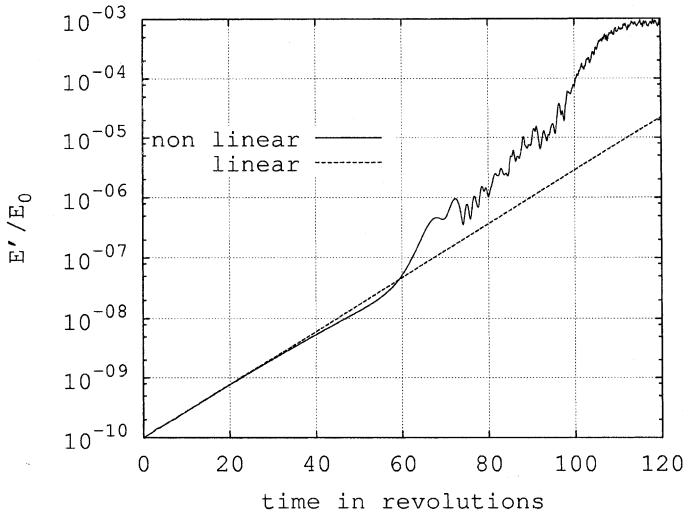

Fig. 9. $Re = 3000$; subcritical bifurcation.

7.2. $Re < 3000$

Similar computations were performed for lower Reynolds numbers, $Re = 2000$ and 2500. The temporal evolutions of E'/E_0 are reported on Fig. 10 for various levels of kinetic energy of the initial condition. These computations show that, for the solution to return to the steady state, the energy level of the initial perturbation has to be extremely small, as low as 10^{-15} times the base flow energy, thereby confirming that this state is stable with respect to infinitesimal perturbations, but unstable to finite amplitude perturbations. However, from a practical point of view, this stability is virtually meaningless because of the actual noise that is always present in experiments or in computations.

From these numerical experiments, we may conclude that the bifurcation (in the discrete sense) does not behave as if it was supercritical. In particular, within the numerical context, it was never possible to obtain in the close vicinity of the linear threshold a small amplitude mono-periodic solution. However, despite that the other facts tend to indicate a subcritical nature of the bi-

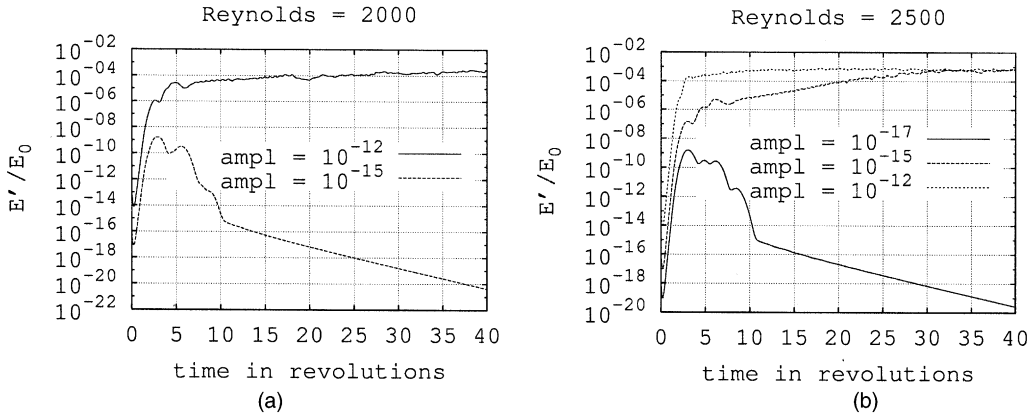

Fig. 10. Temporal evolution of the energy of the fluctuations; subcritical case.

furcation, we are aware that these computations do not constitute a definite proof of it, but rather a probability. In particular, a careful study of the grid influence has to be made. Concerning this last point, preliminary computations have shown that as it could be expected, the different thresholds were shifted when the grid size was varied whereas the qualitative behaviors of the flow were not affected. We would like to remind here that the grid is already a huge one and that a systematic study of the grid influence is virtually impossible to carry out.

7.3. Calculation of the spectrum

7.3.1. Eigenvalues

A limited number of leading eigenvalues of the linearized NS equations are computed by means of the ARPACK package which is based on the use of an implicitly restarted Arnoldi method [11]. As for the computation of the steady state, it is only required to be able to compute the action of the operator on a vector. Details on the method and on the package may be found in Ref. [12].

On Fig. 11 the leading part of the spectrum of the linearized NS operator for $Re = 2900$ and 3000 are shown. They both exhibit an isolated pair of eigenvalues. This pair crosses the imaginary axis for a Reynolds number in the range [2900,3000], in agreement with the linearized calculations of the previous section, thereby confirming the linear threshold. However, the fact that an isolated pair crosses the imaginary axis could lead us to expect a transition to a mono-periodic flow, which is not the case as explained in Section 4. This is clearly seen on Fig. 10.

7.3.2. Eigenmodes

In order to try to get a better insight into what actually happens, it may be useful to look at the structures of some eigenmodes, in particular the mode corresponding to the leading eigenvalue and its first and second harmonics. The iso-v lines of these three modes are displayed on Figs. 12–14. We have also reported on Fig. 15 an instantaneous snapshot of the iso-v lines of the fluctuating velocity in a non-linear computation. These figures do not show any clear connection between the spatial structure of the large amplitude branch and the spatial structures of the most unstable modes. In particular, the structures which appear in the lower right corner of Fig. 15 are not

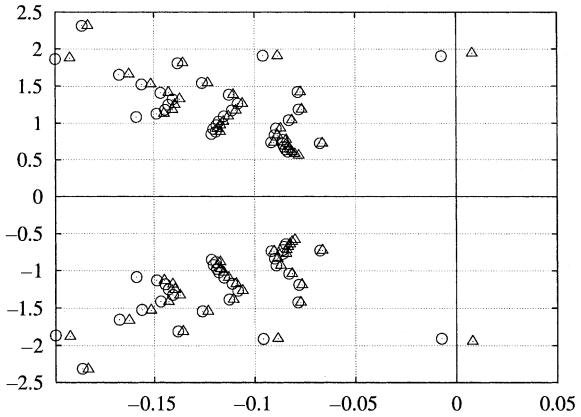

Fig. 11. Spectra of the linearized NS operator for (◯) $Re = 2900$ and (△) $Re = 3000$.

Fig. 12. The unstable mode.

Fig. 13. First harmonic of the unstable mode.

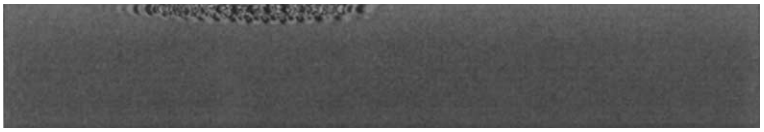

Fig. 14. Second harmonic of the unstable mode.

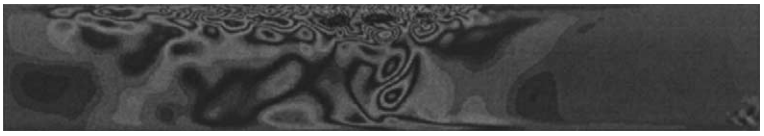

Fig. 15. Instantaneous v-mode.

present in any of the three eigenmodes which are displayed and the spatial extension of the structures along the stator for the non-linear case is more important than for the eigenmodes. Moreover, the latter exhibits higher frequencies than the former, a fact which is evidenced on

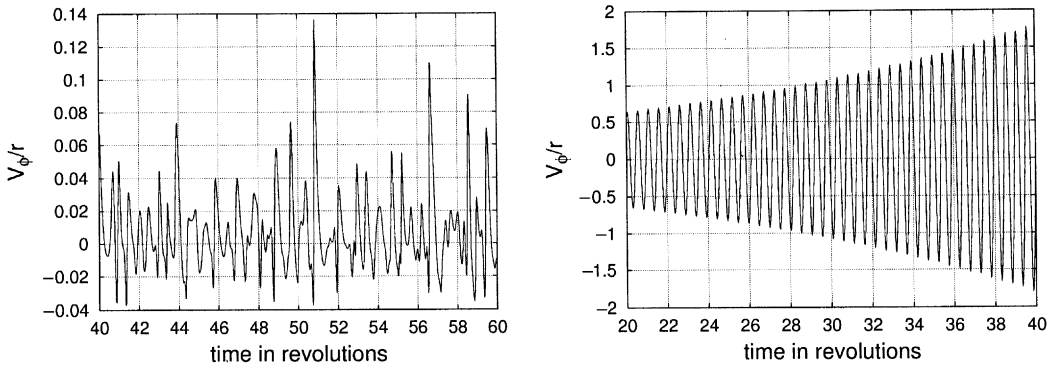

Fig. 16. Time evolution of v/r close to the stator in the non-linear and linear case, $Re = 3000$.

Fig. 16 which displays the time evolution, in the non-linear and linear cases, of the local angular velocity v/r at a point located close to the fixed disk and at a distance $= R_0/5$ from the axis.

8. Conclusion

We have developed a general methodology to investigate flow instabilities in enclosures. This methodology allows for the determination of the linear stability criteria and of the leading eigenmodes of flows in enclosures. It further allows one to investigate the nature (sub or super-critical) of the corresponding bifurcation. This methodology was applied to the so-called rotor–stator disk flow of radial aspect ratio 10 and the computations indicate that the first bifurcation of the Batchelor's type solution presents many subcritical features. We have further shown that there exists a large amplitude chaotic branch which extends far below the critical value and onto which solutions are inevitably attracted due to the large non-normality of the Jacobian linearized evolution operator. The question of the possible connection of the large amplitude branch to the unstable branch coming from the bifurcation point remains unanswered.

References

[1] Cousin-Rittemard N, Daube O, Le Quéré P. Sur la nature de la première bifurcation des écoulements interdisque. CRAS Série IIb 1998;326(6):359–66.
[2] Cousin-Rittemard N, Daube O, Le Quéré P. Description des couches limites des écoulements stationnaires interdisques en configuration rotor–stator. CRAS Série IIb 1999;327(6):215–20.
[3] Cousin-Rittemard N, Daube O, Le Quéré P. Structuration de la solution stationnaire des écoulements interdisques en configuration rotor–stator. CRAS Série IIb 1999;327(6):221–6.
[4] Jacques R, Le Quéré P, Daube O. Comparaisons entre simulations directes et modélisation k–ϵ pour les écoulements en configuration rotor–stator. Revue Générale de Thermique 1998;7(7):567–81.
[5] Elena L, Schiestel R. Turbulence modeling of confined flow in rotating disk systems. AIAA J 1995;33(5):812–21.
[6] Le Quéré P, Behnia M. From onset of unsteadiness to chaos in a differentially heated square cavity. J Fluid Mech 1998;359:81–107.

[7] Daube O. Numerical simulation of axisymmetric vortex breakdown in a closed cylinder. In: Lectures in applied mathematics, vol. 28. AMS; 1991. p. 131–52.
[8] Daube O, Le Quéré P, Cousin-Rittemard N, Jacques R. Influence of curvature on transition to unsteadiness and chaos of rotor–stator disk flows. J Fluid Mech, submitted for publication.
[9] Vanel JM, Peyret R, Bontoux P. A pseudo-spectral solution of vorticity–stream-function equations using the influence matrix technique. In: Num Meth Fluid Dyn II. Oxford: Clarendon Press; 1986. p. 463–75.
[10] Haidvogel DB, Zang T. The accurate solution of Poisson's equation by expansions in Chebychev polynomials. J Comp Phys 1979;30:167–80.
[11] Sorensen DC. Implicit application of polynomial filters in a k-step Arnoldi method. SIAM J Matrix Anal A 1992;13:357–85.
[12] Lehoucq RB, Sorensen DC, Yang C. ARPACK user's guide. Philadelphia: SIAM; 1998.
[13] Saad Y, Schultz MH. GMRES: a generalized minimal residual algorithm for solving nonsymmetric linear systems. SIAM J Sci Stat Comp 1986;7:856–69.
[14] Trefethen LN. Pseudo-spectra of linear operators. SIAM Rev 1997;39:383–406.
[15] Mamum CK, Tuckerman LS. Asymmetry and Hopf bifurcation in spherical Couette flow. Phys Fluids 1995;7: 80–91.
[16] Tuckerman LS. Steady-state solving via Stokes preconditioning: recurrence relations for elliptic operators. In: Dwoyer DL, Hussaini MY, Voigt RG, editors. Lecture notes in physics. New York: Springer; 1989. p. 573.